Photoionization of H_2^+ beyond the dipole approximation with zeptosecond time resolution

Zhao-Han Zhang[1] and Feng He[1,2,*]

[1]*Key Laboratory for Laser Plasmas (Ministry of Education) and School of Physics and Astronomy, Collaborative Innovation Center for IFSA (CICIFSA), Shanghai Jiao Tong University, Shanghai 200240, China*

[2]*CAS Center for Excellence in Ultra-intense Laser Science, Shanghai 201800, China*

(Received 9 February 2021; accepted 11 March 2021; published 19 March 2021)

We numerically simulate the photoionization of a hydrogen molecular ion exposed to a monochromatic extreme ultraviolet laser field beyond the dipole approximation. In such a diatomic system, the laser field reaches the two nuclei at different instants, adding extra phase on the ionization events from two nuclei and resulting in the shift of the angular maxima in the photoelectron momentum distribution. In the limit of the infinite internuclear distance, the double-slit interference scenario can be adopted to explain the simulated photoelectron momentum distribution. However, when the internuclear distance is as short as 1 Å, the electron distributes more in the center of the molecule, and the photoelectron momentum distribution carries the single-slit diffraction character. The extracted birth time delay of photoemission from two nuclei is about a few hundred of zeptoseconds, which is similar to the experimental measurement in H_2 [Grundmann *et al.*, Science **370**, 339 (2020)].

DOI: 10.1103/PhysRevA.103.033112

I. INTRODUCTION

Exposing an atom or molecule to a light pulse whose photon energy is larger than the ionization potential of the target, the ionization happens. Such a scenario has been explained by Einstein's photoelectric effect. With the advent of ultrashort laser technology, the phenomena of multiphoton and tunneling ionization have been well accepted. Photoionization is the most fundamental process and plays the central role in ultrafast physics [1]. In photoionization, the quiver radius of electron in laser fields is much smaller than the laser wavelength, therefore the dipole approximation is adopted. Within the dipole approximation, the photon momentum is neglected, and the photoelectron momentum alongside the laser propagation is symmetric with respect to zero. Though the nondipole effect that the longitudinal momentum distribution is shifted was predicted years ago [2], it was not until 2011 that Smeenk *et al.* [3] experimentally measured the photoelectron momentum along the laser propagation acquired from a circularly polarized light. This study was followed by other experimental works on the photon-photoelectron momentum transfer [4–6] as well as theoretical analysis. In the tunneling ionization driven by a circularly polarized laser pulse, the averaged photoelectron longitudinal momentum (along the laser propagation direction) is roughly about E_k/c, where E_k is the photoelectron kinetic energy and c is the light speed. *Ab initio* simulation and recently experimental measurement showed that the longitudinal momentum should be $E_k/c + \frac{1}{3}I_p/c$ [7–10]. If the tunneling ionization is induced by a linearly polarized laser pulse, the rescattering plays a crucial role. In this case, the interplay of the Coulomb potential [11] and the magnetic component in the laser pulse together govern the electron longitudinal momentum distribution [12]. On the other hand, in the single-photon ionization, the behavior of the ionized wave packet is quite different compared to that of tunneling ionization. To be specific, the quiver radius and ponderomotive energy are much smaller, therefore, the recollision process is insignificant. The longitudinal momentum distribution modified by the Coulomb potential is of minor importance. The averaged photoelectron longitudinal momentum in single-photon ionization is $\frac{8}{5}E_k/c$, and the nucleus acquires the longitudinal momentum $-\frac{3}{5}E_k/c + I_p/c$ [13]. In a more complex process such as single-photon double ionization, the photon momentum may be shared between two electrons and one nucleus [14].

Compared to atoms, the multiple Coulomb centers of molecules bring more intriguing scenarios. For its simplicity, H_2^+ has worked as a prototype for understanding molecular ionization and dissociation [15–17]. In the dipole approximation, photoemission from each nucleus in H_2^+ happens synchronously, and thus the constructive interference in the photoelectron momentum distribution appears at angles α satisfying $\cos\alpha = 0$, and the adjacently constructive peaks are separated by $2\pi/R$ [18,19], where α is the cross angle between the electron momentum and molecular axis. After considering the nondipole effect, the laser pulse may reach the two nuclei at different times, which brings an extra phase difference in the ionization events from the two nuclei. As explored by Grundmann *et al.* in a recent experiment [20], the interference patterns of the single-photon ionization of H_2 tilt, and the constructive interference appears at α_n satisfying $pR\cos(\alpha_n) - \frac{p^2}{2}\tau_b = 2\pi n, n = 0, \pm 1, \ldots$, with τ_b the propagation time of light from one nucleus to the other, p is the magnitude of the photoelectron momentum, and R is the internuclear distance. Inversely, by measuring the location of the angular maxima, one can extract τ_b.

*fhe@sjtu.edu.cn

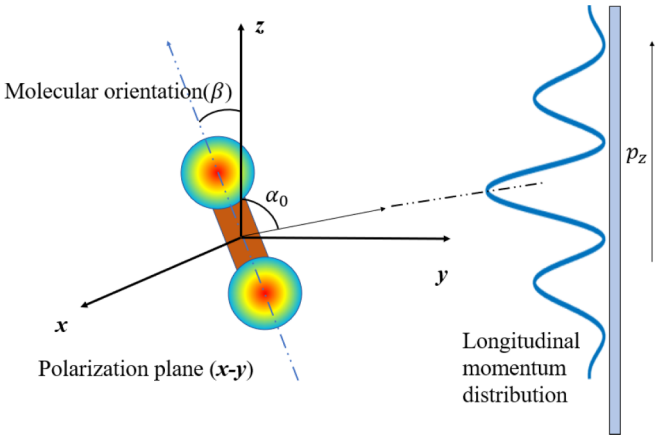

FIG. 1. The schematic of the physical process. The H_2^+ is exposed to an XUV laser pulse, whose propagation direction $\boldsymbol{k}$ is fixed at the z direction, and the polarization direction is within the x-y plane. The molecular axis can have a fixed angle β to the z axis. The longitudinal momentum distribution of the ionized electron wave packet exhibits a double-slit interference structure, and the angle α_0 indicates the location of the maximum photoelectron angular distribution.

In this paper, we systematically study the laser propagation time between the two nuclei in H_2^+ based on the photoionization of H_2^+ in strong extreme ultraviolet (XUV) fields. By numerically simulating the time-dependent Schrödinger equation (TDSE) for H_2^+ with different bond lengths, we obtain the photoelectron momentum distribution, from which the time delay of photoemission from the two nuclei is extracted. In the ultimate case when R tends infinity, the extracted birth time delay is R/c. On the other hand, when R approaches 0, such a time delay is about $4R_s/c$, where R_s is the effective distance for the photon to travel through the molecule. The TDSE simulation results are supported by the nondipole strong field approximation (NSFA). The rest of the paper is organized as follows. In Sec. II we introduce the numerical method. The results and analyses are presented in Sec. III. The paper ends with a conclusion in Sec. IV.

II. NUMERICAL METHODS

We study the photoionization of H_2^+ in a strong XUV laser field as shown in the schematic Fig. 1. The vector potential $\boldsymbol{A}$ has the form

$$\boldsymbol{A}(\eta) = f(\eta)[A_0\cos(\omega\eta)\boldsymbol{e}_x + A_0\sin(\omega\eta)\boldsymbol{e}_y], \tag{1}$$

where $\eta = t - \boldsymbol{n}\cdot\boldsymbol{r}/c$ is the light cone time, $f(\eta) = \sin^2(\pi t/T)$ is a sine square envelope function with a duration T of 20 optical cycles in numerical calculation or equals one in theoretical analysis, and ω is the central angular frequency. In this paper, the laser propagates along the z axis, namely, $\boldsymbol{n} = (0, 0, 1)$. The ionization process is governed by TDSE (atomic units are used throughout unless stated otherwise),

$$i\frac{\partial}{\partial t}\Psi(t,\boldsymbol{r}) = \left\{\frac{1}{2}[\hat{\boldsymbol{p}} + \boldsymbol{A}(\eta)]^2 + V(\boldsymbol{r})\right\}\Psi(t,\boldsymbol{r}), \tag{2}$$

where $\boldsymbol{r}$ is the electron coordinate. The Coulomb potential is expressed as

$$V(\boldsymbol{r}) = -\frac{1}{|\boldsymbol{r} - \boldsymbol{R}/2|} - \frac{1}{|\boldsymbol{r} + \boldsymbol{R}/2|}. \tag{3}$$

The internuclear distance R is a parameter instead of a dynamical variable, and the molecular axis is fixed alongside the z axis unless stated otherwise. One can go back to the dipole case by simply replacing η with t in Eq. (2). By using $\boldsymbol{r} = (x, z)$, Eq. (2) is solved numerically on a two-dimensional rectangular grid with 16 384 × 16 384 grid points in total. The grid steps are 0.0625 a.u. A second-order implicit Crank-Nicolson method combined with a corresponding split-operator scheme [21–23] is taken to evolve the wave function. In each laser cycle, 1800 times of propagation with equal time steps are performed. To match the ground state energy of the two-dimensional model to the real case, an R-dependent soft-core parameter $\alpha(R)$ is used and $V(x,z) = [x^2 + (z - R/2)^2 + \alpha(R)]^{-1/2} + [x^2 + (z + R/2)^2 + \alpha(R)]^{-1/2}$. The wave function is freely propagated after the laser is turned off until the main body of the singly ionized wave packet travels far enough from the Coulomb center. The simulation box is big enough to hold all ionized states such that no absorber is set around the numerical boundaries. The momentum distribution is then extracted by doing Fourier transformations to the ionized wave packet. Such a method is proved to be equivalent to projecting onto the exact Coulomb scattering states if the wave packet travels far enough [24].

While the TDSE numerical simulation gives accurate wave functions, the physical mechanism is not as transparent as explored by the nondipole strong field approximation (NSFA) [11]. In NSFA, the photoionization amplitude is expressed as

$$M(\boldsymbol{p}, b) = \int_0^T \boldsymbol{W}(\eta)\cdot\nabla\tilde{\phi}_b[\boldsymbol{q}(\eta)]e^{iS_p(\eta)+iI_p\eta}\,d\eta, \tag{4}$$

where the nondipole Volkov phase is

$$S_p(\eta) = \int_{\eta_i}^{\eta}\left[\frac{1}{2}\boldsymbol{p}^2 + \frac{\boldsymbol{A}(\eta')\cdot\boldsymbol{p} + \frac{1}{2}\boldsymbol{A}^2(\eta')}{1 - \frac{p_z}{c}}\right]d\eta', \tag{5}$$

and the ionization potential I_p is a function of R. The prefactor $\boldsymbol{W}(\eta)$ in Eq. (4) is

$$\boldsymbol{W}(\eta) = -\left(1 - \frac{p_z}{c}\right)\frac{\partial\boldsymbol{A}(\eta)}{\partial\eta}. \tag{6}$$

The canonical momentum is expressed as

$$\boldsymbol{q}(\eta) = \boldsymbol{p} + \boldsymbol{A}(\eta) - \left(\frac{\boldsymbol{p}^2}{2c} + \frac{I_p}{c}\right)\boldsymbol{n}. \tag{7}$$

In the above expressions, by setting c to be infinite and hence neglecting the term $O(\frac{1}{c})$, we regress to the SFA within the dipole approximation. $\tilde{\phi}_b(\boldsymbol{q}(\eta))$ at $t = 0$ is the three-dimensional ground state of H_2^+ in momentum representation. At $R = 0$, the initial state is analytically expressed in terms of the Gegenbauer polynomials and the spherical harmonics [25]. For arbitrary R, it can be obtained accurately by the Killingbeck method as described in Ref. [26]. The integrals of Eqs. (4) and (5) are performed by explicit Euler

summations with more than 2000 time steps in each laser cycle, which sufficiently suppresses the numerical error induced by the fluctuation of the integrand.

Besides starting from an accurate $\tilde{\phi}_b$ as described above, we also solved the problem in a simplified model by assuming the initial state to be a linear combination of atomic orbitals $\Psi(t=0,\boldsymbol{r}) \propto (e^{-Z|\boldsymbol{r}-\boldsymbol{R}/2|} + e^{-Z|\boldsymbol{r}+\boldsymbol{R}/2|})$, where $Z = Z(R)$ is an effective nuclear charge parameter. For $R \to 0$ as the united atom picture, one may expect $Z \to 2$, and for $R \to \infty$, the separated atoms picture requires $Z \to 1$. For intermediate cases, the value $I_p(R) = Z^2(R)/2$ is used for simplification. Such an analytic procedure is also seen in Ref. [27]. In this assumption, Eq. (4) gives an analytic expression in the weak-field limit $A_0 \to 0$. The starting point is the Fourier transform of the wave function

$$\tilde{\phi}_b(\boldsymbol{q}) \propto \frac{1}{(Z^2+\boldsymbol{q}^2)^2}\cos\left(\frac{1}{2}\boldsymbol{q}\cdot\boldsymbol{R}\right). \tag{8}$$

After taking the limit $A_0 \to 0$, $\boldsymbol{q}(\eta) \to \boldsymbol{p} - (p^2/2 + Z^2/2)\boldsymbol{n}$, $S_p(\eta) \to p^2\eta/2$, for $f(\eta) = 1$, Eq. (4) is reduced to

$$\begin{aligned}
|M(\boldsymbol{p},b)|^2 &\propto \left|\int_{-\infty}^{\infty} d\eta e^{i(p^2/2+I_p-kc)\eta}\left(1-\frac{p_z}{c}\right)\left(\frac{\partial}{\partial p_x}+i\frac{\partial}{\partial p_y}\right)\tilde{\phi}_b(\boldsymbol{q})\right|^2 \\
&\propto \delta^2\left(\frac{p^2}{2}+I_p-kc\right)\frac{[1-\frac{p}{c}\cos(\alpha_0)]^2 p^2\sin(\alpha_0)^2}{[p^2+k^2+Z^2-2pk\cos(\alpha_0)]^6}\cos^2\left[\frac{pR\cos(\alpha_0)-kR}{2}\right] \\
&\propto \delta^2\left(\frac{p^2}{2}+I_p-kc\right)\frac{[1-\frac{p}{c}\cos(\alpha_0)]^2\sin(\alpha_0)^2}{\left[1-\frac{2pk}{p^2+k^2+Z^2}\cos(\alpha_0)\right]^6}\{1+\cos[pR\cos(\alpha_0)-kR]\} \\
&\propto \delta^2\left(\frac{p^2}{2}+I_p-kc\right)\frac{1-\cos^2(\alpha_0)}{[1-\nu_c\cos(\alpha_0)]^4}\{1+\cos[\nu_p\cos(\alpha_0)-\nu_k]\}+O(c^{-2}).
\end{aligned} \tag{9}$$

Here $k = \omega/c$ is the photon momentum, and $\nu_c = 2pk/(p^2 + k^2 + Z^2)$, $\nu_p = pR$, $\nu_k = kR$ are dimensionless constants once ω and R are fixed. One can immediately identify that $\nu_c = p/c + O(c^{-2})$ by substituting $\omega = p^2/2 + I_p = (p^2 + Z^2)/2$. We thus ignore ν_c^2 and higher order terms to obtain the last line in Eq. (9). We also point out that ν_k/ν_p is of c^{-1} order. By taking derivatives with respect to $\cos(\alpha_0)$ and ignoring c^{-2} and higher order terms, the central maxima is determined by

$$\nu_p\tan\left[\frac{\nu_p\cos(\alpha_0)-\nu_k}{2}\right] - \frac{2\cos(\alpha_0)}{1-\cos^2(\alpha_0)} + 4\nu_c = 0. \tag{10}$$

In the limit of $R \to \infty$,

$$\cos(\alpha_0) = \frac{\nu_k}{\nu_p} + \frac{4\nu_k}{\nu_p^3} - \frac{8\nu_c}{\nu_p^2} + O(R^{-4}), \tag{11}$$

and in the limit of $R \to 0$,

$$\cos(\alpha_0) = 2\nu_c\left(1+\frac{\nu_p^2}{4}\right) - \frac{\nu_p\nu_k}{4} + O(R^4). \tag{12}$$

Equations (11) and (12) imply that near $R = 0$, $\cos(\alpha_0)$ is located at the limit of $4E_e/pc$, and that at $R = \infty$, it asymptotically tends to $(E_e + I_p)/pc$. Another prediction of Eqs. (11) and (12) is that when $\omega < 4I_p/3$, which is possible in the case of relatively low-energy single-photon ionization, the monotonicity of $\cos(\alpha_0)$ with respect to R is reversed.

III. RESULTS

The double-slit interference in photoionization of the diatomic molecules in the dipole approximation has been widely studied [28–30], where the longitudinal momentum distribution is symmetric with respect to the plane $p_z = 0$. Once the nondipole effect is taken into account, the photoelectron momentum distribution shifts alongside the direction of the photon momentum by a small amount. In our simulations, the laser propagation direction is parallel to the molecular axis. For TDSE, after obtaining the photoelectron wave packet in momentum representation $\phi(p_x, p_z)$, we calculate the longitudinal momentum distribution $W(p_z) = \int |\phi(p_x, p_z)|^2\, dp_x$. For SFA and NSFA, the longitudinal momentum distribution is evaluated by $W(p_z) = \int |M(p_x, p_y, p_z)|^2\, dp_x\, dp_y$, which is shown in Figs. 2(a) and 2(b) at $R = 2$ a.u. and $R = 10$ a.u., respectively. Similar momentum shifts have been explored in molecular systems and atomic systems [31–35]. Note that the shift of the expected momentum and the most probable momentum could be opposite if the Coulomb potential plays a role in the rescattering process [31,36,37].

To reveal the relation between R and $\cos(\alpha_0)$, we numerically calculated the momentum shift of the central maximum of the longitudinal momentum distribution at various R. To obtain that, we have fitted the longitudinal momentum distribution with a Gaussian function at small R and a cosine function at moderate R. The longitudinal momentum distribution takes values on a set of p_z grid points with equal spacing δp_z less than 0.01 a.u. to obtain smooth fitting curves. In both cases, the $\mathcal{R}^2$ of the fittings are larger than 0.99 by choosing the proper ranges of p_z.

Figure 3 shows the momentum shift Δp_z along the laser propagation direction. Here Δp_z is formally defined by the point satisfying $dW(p_z)/dp_z|_{\Delta p_z} = 0$. Actually, Δp_z is the displacement of the central peak of $W(p_z)$ to the right side of $p_z = 0$. Δp_z decreases monotonically with the increase of R and reaches the asymptotic value $(E_k + I_p)/c$, as indicated by the dashed blue line. Such asymptotic behavior at large R follows exactly what Eq. (11) predicts. The I_p/c term is attributed to the dynamical phase accumulated on the electron's

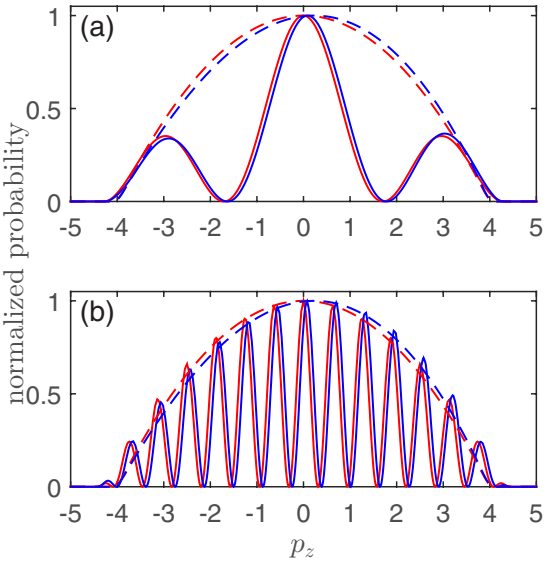

FIG. 2. Solid lines: The longitudinal momentum distributions for (a) $R = 2$ a.u. and (b) $R = 10$ a.u. Dashed lines: the longitudinal momentum distributions for the photoelectron of the hydrogen atom for reference, where the unit of p_z is a.u. The lines being symmetric with respect to $p_z = 0$ a.u. are the results calculated by SFA within the dipole approximation, whereas the lines shifted to the right side are the results calculated by NSFA. The maxima of the distributions are normalized to 1. The laser parameters are $\omega = 10$ a.u., $T = 20$ optical cycles, $A_0 = 0.01$ a.u. The molecular orientation is fixed at the z direction.

bound state. Neglecting the I_p/c phase in a more simplified double-slit model will cause an 8% deficit to the final result in the simulation using $\omega = 10$ a.u. If a sufficiently high driving frequency is used instead, such neglect is then apparently

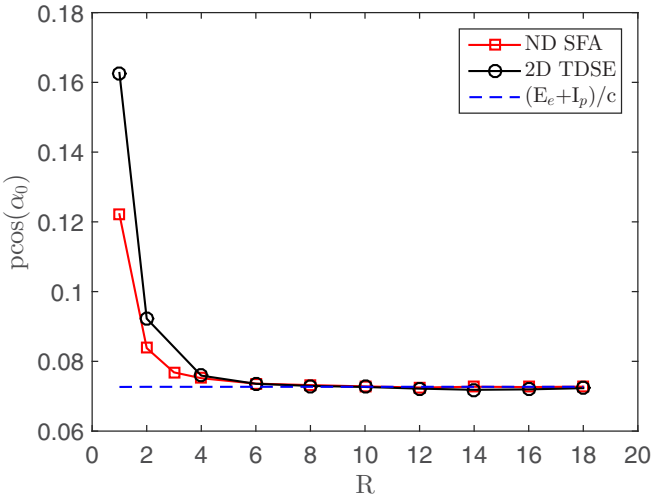

FIG. 3. The central maximum of the longitudinal momentum distribution as a function of R in atomic units. The black circles and red squares are results calculating by TDSE and NSFA, respectively. The blue dashed line is the results predicted by (11). The laser parameters are $\omega = 10$ a.u., $T = 20$ optical cycles, $A_0 = 1.0$ a.u. for TDSE, and $A_0 = 0.01$ a.u. for NSFA. The molecular orientation is fixed at the z direction.

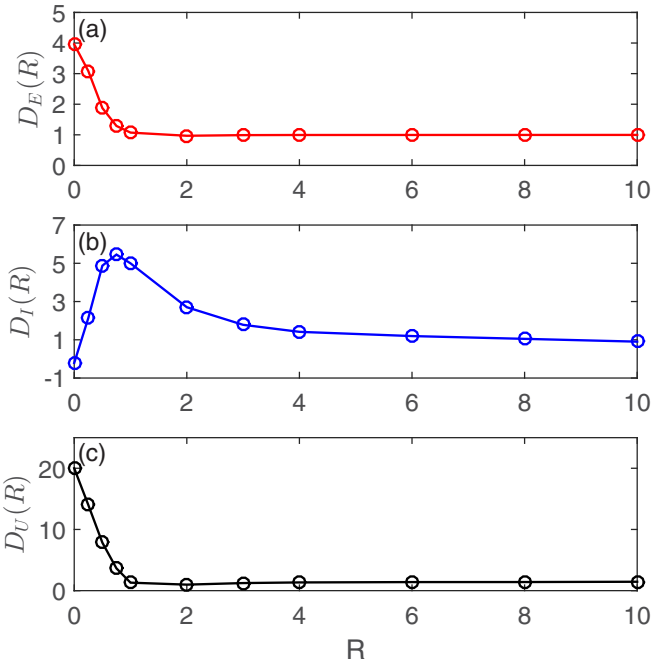

FIG. 4. Fitted coefficients (a)D_E,(b)D_I,(c)D_U as functions of R in atomic units. Their definitions are found in text. The molecular orientation is fixed at the z direction.

acceptable. For small R, the momentum shift significantly deviates from $(E_k + I_p)/c$ due to the deformation of the initial state wave function. In this case, the initial wave packet distributes more in the middle of the two nuclei, in which case the single-slit diffraction is more proper than the double-slit interference to be used to explain the calculation results.

The numerical simulation results of TDSE can be reproduced by the NSFA. In Fig. 3, the black solid line with circles presents the R-dependent Δp_z given by the NSFA model, while the red solid line with squares indicates the same quantity given by TDSE. The good agreement between the two models confirms that the long-range effects of the Coulomb potential is negligible for explaining the observed results in single-photon ionization. Please note that the Coulomb potential is very important for producing the correct longitudinal momentum distribution in tunneling ionization [12,36,37].

The deviation of the simulation results to the theoretical expectation $(E_k + I_p)/c$ impels us to find a general expression to describe the momentum shift. As Δp_z depends on the photon momentum and ionization potential as well as ponderomotive energy, we model Δp_z,

$$\Delta p_z = \frac{D_E(R)E_e + D_I(R)I_p(R) - D_U(R)U_p}{c}. \quad (13)$$

Here D_E, D_I, D_U are three dimensionless coefficients depending only on R. To numerically obtain D_E at a fixed value of R, one shall vary the laser frequency and intensity simultaneously in order to keep U_p unchanged. After a data set of $(E_e, \Delta p_z)$ at given R is obtained, one can linearly fit the data set and extract the slope D_E as well as the intercept $D_I I_p - D_U U_p$. By repeating the procedure with different U_p, one can immediately obtain the slope D_U as well as D_I. Figure 4 presents the extracted R-dependent coefficients. The laser fre-

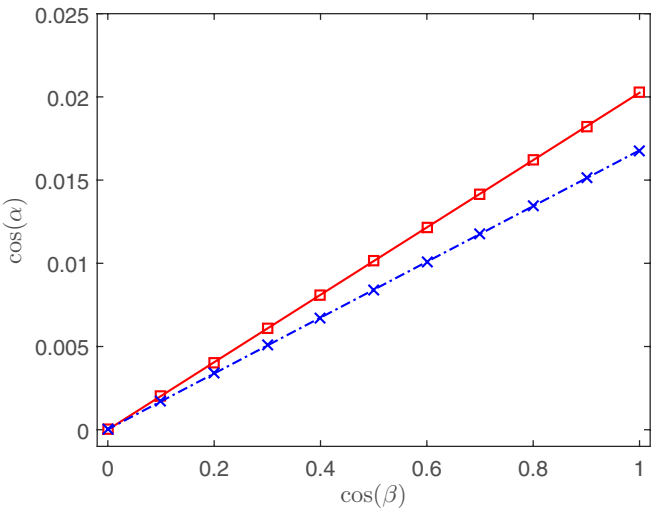

FIG. 5. The dependence of $\cos(\alpha)$ on $\cos(\beta)$ for $R = 2$ a.u. (red line with squares) and $R = 10$ a.u. (blue line with crossings), where β is the angle between molecular axis and laser propagation. Laser parameters are $\omega = 10$ a.u., 20 cycles, $A_0 = 0.02$ a.u.

quencies used in each fit range from 6 to 20 a.u. As shown in Fig. 4(a), D_E decreases with the growth of R. The limit values $D_E(0) = 4, D_I(0) = 0$ and $D_E(\infty) = 1, D_I(\infty) = 1$ follow exactly what (12) and (11) have predicted. One can note that a peak occurred in Fig. 4(b) near $R = 1$, which may be mainly induced by the rapid deviation of I_p from that of He^+. These coefficients become stable when $R > 4$ a.u. This indicates the double-slit interference picture works well when $R > 4$ a.u., whereas at $R < 4$ a.u. the mixture of single-slit diffraction and double-slit interference play roles in the photoionization.

When the laser propagation direction has a crossing angle of β to the molecular axis, the laser wavefront will see an effective bond length $R\cos(\beta)$. One can expect that the location of the angular maximum depends on β. Figure 5 shows the dependence of $\cos\alpha$ on $\cos\beta$ for the case of $R = 2$ a.u. (red solid line) and $R = 10$ a.u. (blue dashed line). Since a larger $\cos\beta$ corresponds to a longer effective bond length, a larger Δp_z appears at a smaller β.

IV. CONCLUSIONS

Both the TDSE and the NSFA calculations explore that the laser wavefront reaches the two nuclei in H_2^+ at different times in the photoionization, and thus the electron emitted from the two nuclei carries intrinsic different phases. Therefore, the interference of the emitted electron wave packets from the two nuclei leads to the asymmetric longitudinal momentum distribution. The double-slit interference and single-slit diffraction can be used to explain the photoelectron angular distribution when R approaches infinity or zero. The location of the angular maxima depends on the photon momentum, molecular bond length, and laser incident angle. From the photoelectron angular distribution, the photoionization with the zeptosecond time resolution is resolved.

ACKNOWLEDGMENTS

This work was supported by Innovation Program of Shanghai Municipal Education Commission (2017-01-07-00-02-E00034), National Key R&D Program of China (2018YFA0404802), and National Natural Science Foundation of China (NSFC) (Grants No. 11925405 and No. 91850203). Simulations were performed on the π supercomputer at Shanghai Jiao Tong University.

[1] F. Krausz and M. Ivanov, Rev. Mod. Phys. **81**, 163 (2009).
[2] H. R. Reiss, J. Opt. Soc. Am. B **7**, 574 (1990).
[3] C. T. L. Smeenk, L. Arissian, B. Zhou, A. Mysyrowicz, D. M. Villeneuve, A. Staudte, and P. B. Corkum, Phys. Rev. Lett. **106**, 193002 (2011).
[4] A. Ludwig, J. Maurer, B. W. Mayer, C. R. Phillips, L. Gallmann, and U. Keller, Phys. Rev. Lett. **113**, 243001 (2014).
[5] J. Maurer, B. Willenberg, J. Daněk, B. W. Mayer, C. R. Phillips, L. Gallmann, M. Klaiber, K. Z. Hatsagortsyan, C. H. Keitel, and U. Keller, Phys. Rev. A **97**, 013404 (2018).
[6] A. Hartung, S. Brennecke, K. Lin, D. Trabert, K. Fehre, J. Rist, M. S. Schöffler, T. Jahnke, L. Ph. H. Schmidt *et al.*, Phys. Rev. Lett. **126**, 053202 (2021).
[7] S. Chelkowski, A. D. Bandrauk, and P. B. Corkum, Phys. Rev. Lett. **113**, 263005 (2014).
[8] M. Klaiber, E. Yakaboylu, H. Bauke, K. Z. Hatsagortsyan, and C. H. Keitel, Phys. Rev. Lett. **110**, 153004 (2013).
[9] E. Yakaboylu, M. Klaiber, H. Bauke, K. Z. Hatsagortsyan, and C. H. Keitel, Phys. Rev. A **88**, 063421 (2013).
[10] A. Hartung, S. Echart, S. Brennecke, J. Rist, D. Trabert, K. Fehre, M. Richter, H. Sann, S. Zeller, K. Henrichs *et al.*, Nat. Phys. **15**, 1222 (2019).
[11] P.-L. He, Di Lao, and F. He, Phys. Rev. Lett. **118**, 163203 (2017).
[12] X. Chen and F. He, J. Phys. B: At. Mol. Opt. Phys. **53**, 174002 (2020).
[13] S. Grundmann, M. Kircher, I. Vela-Perez, G. Nalin, D. Trabert, N. Anders, N. Melzer, J. Rist, A. Pier, N. Strenger *et al.*, Phys. Rev. Lett. **124**, 233201 (2020).
[14] S. G. Chen, W. C. Jiang, S. Grundmann, F. Trinter, M. S. Schöffler, T. Jahnke, R. Dörner, H. Liang, M. X. Wang, L. Y. Peng, and Q. H. Gong, Phys. Rev. Lett. **124**, 043201 (2020).
[15] J. H. Posthumus, Rep. Prog. Phys. **67**, 623 (2004).
[16] M. R. Miller, Y. Xia, A. Becker, and A. Jaroń-Becker, Optica **3**, 259 (2016).
[17] H. Ibrahim, C. Lefebvre, A. D. Bandrauk, A. Staudte, and F. Légaré, J. Phys. B: At. Mol. Opt. Phys. **51**, 042002 (2018).
[18] H. D. Cohen and U. Fano, Phys. Rev. **150**, 30 (1966).
[19] F. He, A. Becker, and U. Thumm, Phys. Rev. Lett. **101**, 213002 (2008).
[20] S. Grundmann, D. Trabert, K. Fehre, N. Strenger, A. Pier, L. Kaiser, M. Kircher, M. Weller, S. Eckart, L. Ph. H. Schmidt *et al.*, Science **370**, 339 (2020).
[21] M. R. Hermann and J. A. Fleck, Jr., Phys. Rev. A **38**, 6000 (1988).
[22] A. D. Bandrauk and H. Shen, Chem. Phys. Lett. **176**, 428 (1991).
[23] X. B. Bian, Phys. Rev. A **90**, 033403 (2014).

[24] L. B. Madsen, L. A. A. Nikolopoulos, T. K. Kjeldsen, and J. Fernández, Phys. Rev. A **76**, 063407 (2007).
[25] B. Podolsky and L. Pauling, Phys. Rev. **34**, 109 (1929).
[26] G. Hadinger, M. Aubert-Frecon and G. Hadingeret, J. Phys. B: At. Mol. Opt. Phys. **22**, 697 (1989).
[27] D. Lao, P. L. He, and F. He, Phys. Rev. A **93**, 063403 (2016).
[28] J. Fernández, O. Fojòn, A. Palacios, and F. Martín, Phys. Rev. Lett. **98**, 043005 (2007).
[29] A. Picòn, A. Bahabad, H. C. Kapteyn, M. M. Murnane, and A. Becker, Phys. Rev. A **83**, 013414 (2011).
[30] X. J. Liu, Q. Miao, F. Gel'mukhanov, M. Patanen, O. Travnikova, C. Nicolas, H. Agren, K. Ueda, and C. Miron, Nat. Photon. **9**, 120 (2014).
[31] S. Chelkowski, A. D. Bandrauk, and P. B. Corkum, Phys. Rev. A **92**, 051401(R) (2015).
[32] A. D. Bandrauk, S. Chelkowski, P. B. Corkum, J. Manz, and G. L. Yudin, J. Phys. B: At. Mol. Opt. Phys. **42**, 134001 (2009).
[33] S. Chelkowski and A. D. Bandrauk, Phys. Rev. A **97**, 053401 (2018).
[34] A. S. Titi and G. W. F. Drake, Phys. Rev. A **85**, 041404(R) (2012).
[35] J. Liu, Q. Z. Xia, J. F. Tao, and L. B. Fu, Phys. Rev. A **87**, 041403(R) (2013).
[36] J. Daněk, M. Klaiber, K. Z. Hatsagortsyan, C. H. Keitel, B. Willenberg, J. Maurer, B. W. Mayer, C. R. Phillips, L. Gallmann, and U. Keller, J. Phys. B: At. Mol. Opt. Phys. **51**, 114001 (2018).
[37] J. Daněk, K. Z. Hatsagortsyan, and C. H. Keitel, Phys. Rev. A **97**, 063409 (2018).